Collision-induced tunneling in methyl halides

H. Harde

Universität der Bundeswehr Hamburg, Holstenhofweg 85, 22043 Hamburg, Germany

R. A. Cheville and D. Grischkowsky

School of Electrical and Computer Engineering and Center for Laser and Photonics Research, Oklahoma State University, Stillwater, Oklahoma 74078

Received March 27, 1997; revised manuscript received June 12, 1997

We use the technique of terahertz time-domain spectroscopy to investigate the absorption and dispersion of spectrally dense methyl halide vapors, particularly in the low- and high-frequency spectral wings. For the first time to our knowledge, it is possible to observe essentially zero-frequency absorption resulting from molecular tunneling between the two states of symmetry simultaneously, with absorption from the entire rotational manifold. We can obtain accurate fits to the measurements on both the low- and high-frequency wings with our new molecular response theory. This theory expands upon the basic van Vleck–Weisskopf and Lorentz theories by assuming a finite reorientation time of a molecule to an external electric field during a collision. This line-shape theory is shown to eliminate the nonphysical Debye plateau of constant absorption at high frequencies inherent in the Debye and van Vleck–Weisskopf theories. © 1997 Optical Society of America [S0740-3224(97)02011-0]

1. INTRODUCTION

We have used the powerful technique of terahertz time-domain spectroscopy[1–9] (THz-TDS) to measure the absorption and dispersion of spectrally dense methyl halide vapors. To match our experiments with theory, we must include an additional small absorption at the low-frequency side of the rotational-band structure. This low-frequency absorption is shown to be due to collision-induced tunneling in symmetric top molecules or equivalently nonresonant absorption that is due to the permanent nonrotating dipole moment.

For these molecules, two states of symmetry, + and −, may be distinguished as representing the two configurations of the molecule with respect to the symmetry or inversion plane determined by the three H atoms. The molecule can switch to its inverse configuration by the tunneling of the carbon-halide group through the symmetry plane.[10,11] The inversion corresponds to a transition between the $+ \leftrightarrow -$ states of the rotational levels, which are split into a degenerate doublet. Unlike the well-known case of the ammonia molecule, in methyl halides the tunneling potential is very high, and therefore the respective tunneling or inversion frequency is extremely low. Unperturbed, the inversion frequency is of the order of nanohertz, corresponding to a period of years. Thus, even at moderate pressures, the linewidth that is due to pressure broadening of such inversion lines is large compared with the center frequency, which can be assumed to be essentially zero. In other words the perturbation experienced by the molecule when it undergoes a collision enables the inversion transition to occur with the corresponding absorption of radiation. Thus only molecular collisions, which cause an almost continuous broadening of the lines up to frequencies in the far infrared, permit measuring the inversion of molecules as a broad background absorption and dispersion. However, measurement of these spectra is complicated by the overlapping rotational band structure of the molecule, which at its maximum is orders of magnitude larger. Therefore only in the far wings of the rotational band can these two contributions be distinguished.

Alternatively the collisionally broadened inversion lines at essentially zero frequency can be considered as a Debye-type absorption that is due to the stationary or nonrotating permanent dipole moment reorienting during a molecular collision.[10,12] In this viewpoint the component of the dipole moment parallel to the total angular-momentum vector realigns during collisions and contributes to the Debye absorption. Formally, this picture is identical with that of the inversion line absorption discussed in the previous paragraph.[10]

With the newly developed terahertz beam sources, producing subpicosecond pulses of terahertz radiation, a new and wide frequency range for time- and frequency-domain studies of molecular vapors is available. The pulses essentially consist of a single cycle over a pulse duration of typically 300 fs and are characterized by a transform-limited white spectrum covering nearly two decades of frequency from approximately 50 GHz up to 5 THz.[9,13] This frequency range, midway between the microwave and infrared frequencies, is important owing both to the samples that can be investigated and to the unique experimental conditions encountered with these terahertz pulses. Previous experimental work on low-frequency absorption has used mainly microwave techniques and focused on frequencies low enough to neglect the contribution of the rotational manifold.[10,11] Furthermore, experimental limitations necessitated that these measurements could be made only at a limited number of discrete frequencies. With our terahertz technique the fact that a

0740-3224/97/123282-12$10.00

continuous band of frequencies can be monitored in a single measurement permits, for the first time to our knowledge, determination of the low-frequency nonresonant or inversion-line absorption simultaneously with the rotational manifold out to the far wings.

Standard collision theory predicts a line shape for a pressure-broadened line with zero transition frequency, which is given by the Debye theory,[14] and is distinguished by a broad, constant absorption and flat phase shift at the higher frequencies. However, such absorption would cause a physically and unacceptably large additional contribution in the high-frequency wing that is in disagreement with our broad bandwidth measurements and cannot completely explain the observed spectrum in the low-frequency wing.

To explain this discrepancy, we have applied our new molecular response theory,[15] which was developed for rotational transitions but also holds for the inversion lines. Compared with conventional collision theories, it additionally includes the molecular response of polar molecules to an external electric field over the duration of a collision. With a response time of the order of 200 fs, as found from analysis of the rotational spectra, the absorption shows a well-restricted maximum at 150 GHz and causes a significant attenuation only in this frequency range, eliminating the nonphysical Debye plateau. With this new line shape, excellent agreement between measurement and calculation is obtained over the full spectral range of our measurements.

2. EXPERIMENTAL SETUP

The optoelectronic terahertz system used for our experiments is shown in Fig. 1. The key element for generating terahertz radiation is a photoconducting chip[13] [Figs. 1(a) and 1(b)] irradiated with 60–70-fs laser pulses coming at a rate of 100 MHz from a Ti:sapphire laser.

Two source geometries are used in this investigation. For experiments investigating the high-frequency wing of the rotational manifold the terahertz source consists of two coplanar transmission lines separated by 80 μm and dc biased with a voltage of 100 V [Fig. 1(a)].[13] When the metal–semiconductor interface of the positively biased line is irradiated with the optical pulses, strong bursts of terahertz radiation are generated. This occurs because photocarriers are created and accelerated in a region of extremely high electric field, the so-called trap-enhanced field. This geometry generates terahertz pulses with frequency components extending from approximately 100 GHz to nearly 5 THz. The terahertz source antenna used for measuring the low-frequency inversion lines had a bow-tie shape [Fig. 1(b)] and was dc biased at 5–10 V. The bow-tie antenna geometry generates pulses with a majority of the spectral-energy density at frequencies below 400 GHz. Thus this source geometry permits measurements to frequencies slightly below 50 GHz.

The emitted terahertz radiation is collimated by a silicon lens and a paraboloidal mirror into a highly directional beam with a 25-mrad divergence. After a 50-cm propagation distance, this beam is focused by an identical combination of mirror and lens onto the receiving antenna [Fig. 1(c)], which is fabricated on an ion-implanted silicon-on-sapphire wafer. The dipole antenna used for the higher-frequency and bandwidth experiments is fabricated on a coplanar transmission line structure with a 5-μm gap and a 10-μm length.[5] The antenna used for the low-frequency studies was a similar dipole structure with a 200-μm length. The electric field of the incoming terahertz pulses induces a voltage across the 5-μm-wide antenna gap and is measured by photoconductively shorting the gap with laser pulses from a detection beam while monitoring the respective photocurrent in the antenna as a function of the time delay between the optical excitation and probe pulses.

Two vapor cells, located as shown in Fig. 1(d), were used. Measurements optimizing sensitivity near the center of the rotational-line manifold on spectrally dense samples were made in a short cell with a path length of 2.27 cm. This cell was equipped with 1-cm thick high resistivity (10 kΩ cm) silicon windows. Silicon is an optimal window material, which is due to its almost complete transparency and lack of dispersion in the terahertz-frequency range.[8] To maximize sensitivity to the much weaker low-frequency absorption in spectrally dense gases, a much longer 38.2-cm-path-length cell was used, with 2-cm-thick high-resistivity-silicon windows. The entire terahertz system is located in an airtight enclosure to mitigate the effects of water vapor on the terahertz beams.[6]

The cells were filled with methyl fluoride or methyl chloride and fitted with capacitance manometer gauges (MKS Baratron) to measure pressures in the range 0–5000 Torr (0–6666 hPa). The cell was evacuated to <1 mTorr with a roughing pump between each series of measurements. Upon filling the cell, adsorption at the cell wall caused slight pressure drops over time. A me-

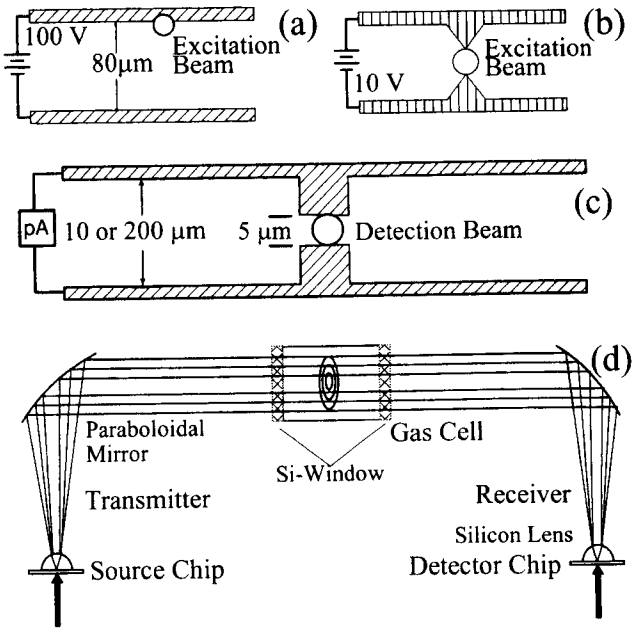

Fig. 1. (a) Optoelectronic transmitting antenna used to generate high-bandwidth pulses of terahertz radiation. (b) Terahertz source antenna for low-frequency experiments. (c) Receiving-antenna geometry. (d) Terahertz collimating and focusing optics together with a vapor cell.

tering valve was used to control cell pressures during data acquisition to ±2.5 Torr (3.33 hPa). The gas was allowed time to come into thermal equilibrium with room temperature after each fill, and a thermocouple sensor accurate within 0.1 K monitored the cell temperature.

3. MEASUREMENTS

We used this optoelectronic terahertz system to perform THz-TDS of methyl halides, which are symmetric top molecules and are interesting candidates for studies of molecular collisions. THz-TDS requires two measurements of the pulse shape, one without the vapor in the cell to determine the input pulse (reference pulse) and another with the vapor in the cell to register the interaction of the pulse with the sample.

Figure 2 shows a measurement for 2000 hPa of methyl chloride in a 2.27-cm-long cell with the system optimized

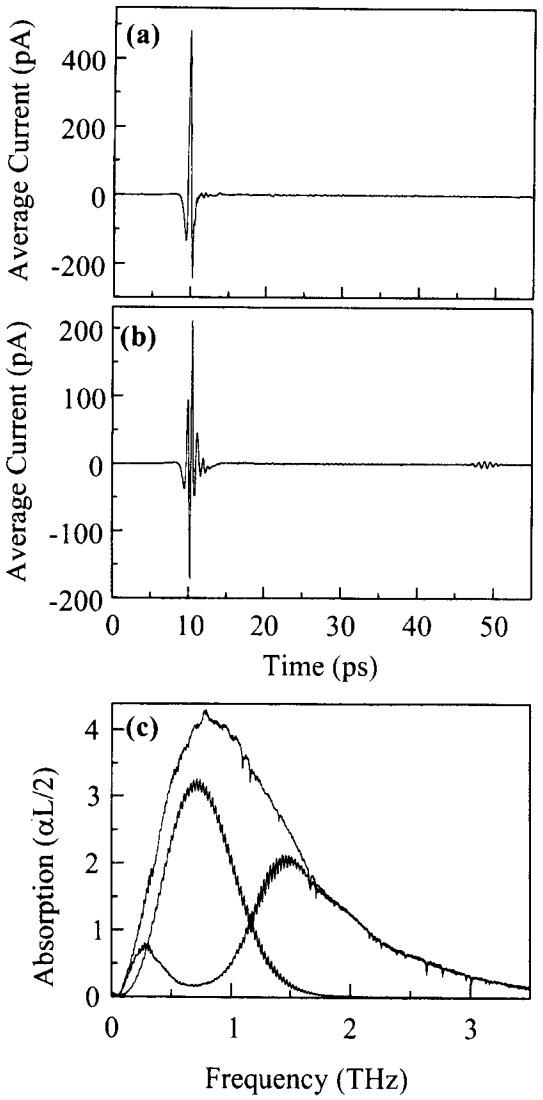

Fig. 2. (a) Measured terahertz pulse without vapor in the cell (input pulse). (b) Terahertz pulse after propagating through a 2.27-cm-long gas cell filled with 2000 hPa of methyl chloride vapor. (c) Fourier-transform spectrum of the input pulse (upper curve), the transmitted pulse (lower curve), and the measured absorption spectrum (middle curve) of methyl chloride.

for high-frequency response (i.e., 10-μm dipole). Despite the short propagation length, the input pulse [Fig. 2(a)] is already strongly reshaped and attenuated at this high pressure and changes to that represented in Fig. 2(b). From the ratio of the Fourier transform of the pulse measured with gas in the cell to that of the reference pulse, the absorption and dispersion of the vapor is found.

The spectrum of the input pulse is shown in Fig. 2(c), as the upper curve in direct comparison with the absorption spectrum of methyl chloride (middle curve), which was derived from the measured pulses of Figs. 2(a) and 2(b). Additionally plotted in Fig. 2(c) is the spectrum of the pulse transmitted through the cell (lower curve). The spectrum of the terahertz pulses extends from low frequencies to almost 5 THz. Thus the central region of the rotational absorption band as well as the low- and high-frequency wings of the band structure can be investigated with high sensitivity and dynamic range. Owing to collisional broadening at this high pressure, the individual lines are already completely overlapped and form an almost continuous broad absorption band.

Because the molecules are excited simultaneously on a multitude of rotational lines, which are distinguished by transitions with an almost constant frequency separation, a periodic rephasing and dephasing of the entire ensemble of more than 70 excited transitions occurs and can be observed in the time domain as terahertz commensurate echoes[1] on the free-induction decay. This echo is seen in Fig. 2(b), occurring at approximately 50 ps. The small magnitude of this echo is due to the rapid collisional dephasing that occurs at 2000 hPa.

At higher pressures and longer propagation lengths the vapor becomes completely opaque at the center of the rotational band but remains partially transparent at the low- and high-frequency wings. Consequently these frequencies may still be investigated with full sensitivity. Figure 3(a) shows a terahertz pulse transmitted through a 38.2-cm-long vapor cell filled with 3039 hPa of methyl chloride, and Fig. 3(b) represents the respective amplitude spectrum (solid curve). The peak amplitude absorption of the rotational manifold is approximately e^{82} or 10^{36} larger in these measurements. The excitation pulse, almost identical to the pulse shown in Fig. 2(a), is completely reshaped and chirped with a fast beating at the leading edge consisting of the transmitted high-frequency components of the spectrum, while the lower frequencies are observed as a small, slow oscillation at the trailing edge of the pulse.

The low-frequency wing of the absorption shown in Fig. 3(b) is enlarged in Fig. 3(c). Figures 3(b) and 3(c) also compare the measurement with the calculated spectrum (dashed curves) of a pulse transmitted through the vapor determined with known molecular constants and considering only the rotational absorption. Good agreement on the high-frequency side is observed when applying the new line-shape theory, which takes into account the time response of molecules aligning to an external electric field in the presence of collisions.[4,15] However, as seen in Fig. 3(c) a large discrepancy is found at the low-frequency side with the data showing absorption a factor of 1.4 greater than predicted by the theory.

This discrepancy can be observed more clearly by tun-

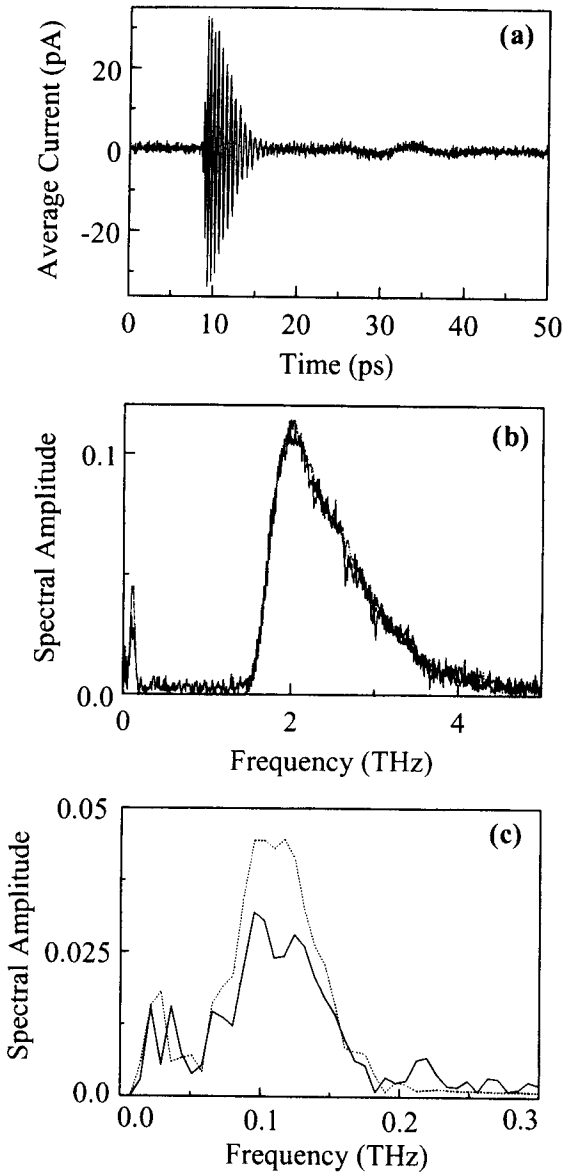

Fig. 3. (a) Measured transmitted terahertz pulse through a 38.2-cm-long gas cell filled with 3039 hPa of methyl chloride vapor. (b) Fourier-transform spectrum of the measured transmitted pulse (solid curve) and calculated amplitude spectrum neglecting inversion (dashed curve). (c) Expanded scale of the data in (b) showing anomalous low-frequency absorption.

ing the optoelectronic terahertz beam system to the low-frequency side of the spectrum. Using the bow-tie terahertz source with a 200-μm dipole detector, we produce the input pulses shown in Fig. 4(a). The amplitude spectrum of the input pulse is shown as an inset to Fig. 4(a). At a pressure of 5512 hPa and a propagation length of 38.2 cm through the vapor the input pulses are reshaped and attenuated as shown in Fig. 4(b) (solid curve). The dashed curve represents a simulated pulse, assuming only the rotational absorption and dispersion. The respective Fourier-transform spectra of the measured (solid curve) and simulated (dashed curve) pulses after transmission through the vapor are shown in Fig. 4(c). The measured transmission at frequencies below cutoff, however, is smaller, and therefore the measured absorption is larger than that calculated by a factor of 1.8; this discrepancy increases with increasing vapor pressure and absorption length. The gas is completely opaque at frequencies above 200 GHz owing to absorption from the rotational manifold.

Similar results on the low-frequency wing are obtained with methyl fluoride at pressures up to 6 atmospheres (6080 hPa). The measured transmitted pulse through 4059 hPa of methyl fluoride with a 38.2-cm path length is shown in Fig. 5(a) together with the pulse structure (upper dashed curve) calculated from rotational absorption and dispersion with use of published constants and the J-dependent linewidth parameters obtained in an earlier investigation.[15] We again see a large discrepancy between measurements and calculations for the calculated amplitude spectrum (upper dashed curve) compared with that measured (solid curve) as shown in Fig. 5(b).

Since the observed deviations from theory for both methyl fluoride and methyl chloride cannot be removed by

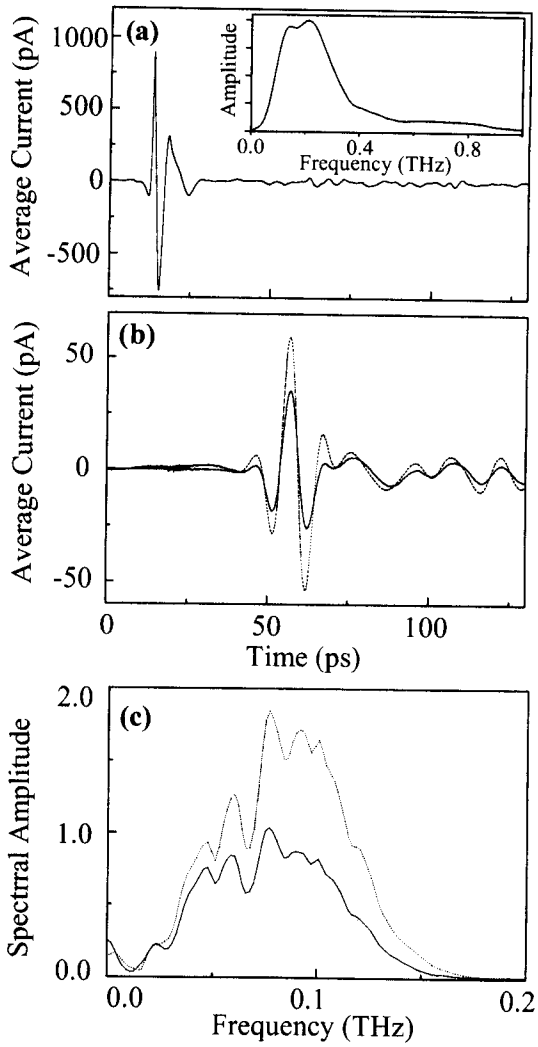

Fig. 4. (a) Input pulse with the optoelectronic terahertz system optimized to low frequencies. The inset shows the amplitude spectrum. (b) Measured transmitted terahertz pulse through a 38.2-cm-long gas cell filled with 5512 hPa of methyl chloride vapor (lower solid curve) and the respective simulation neglecting molecular tunneling (upper dashed curve). (c) Fourier transform spectra of the measured transmitted pulse (lower solid curve) and the simulated pulse (upper dashed curve).

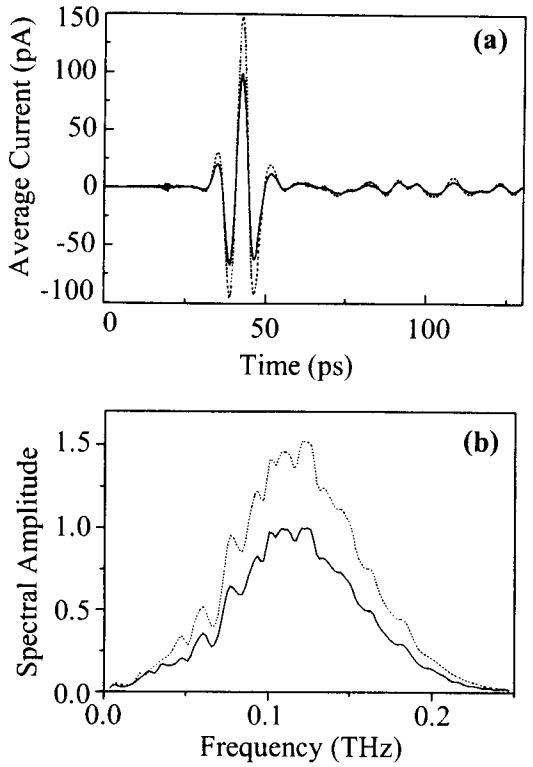

Fig. 5. (a) Measured (lower solid curve) and calculated (upper dashed curve) transmitted terahertz pulse through a 38.2-cm-long gas cell filled with 4059 hPa of methyl fluoride vapor. The input pulse is similar to that shown in Fig. 4(a). (b) Fourier-transform spectrum of measured transmitted pulse (lower solid curve) and calculated pulse (upper dashed curve).

fitting any one of the rotational parameters, we are forced to consider the additional absorption process originating from the tunneling of symmetric top molecules.

4. THEORY

In this section we develop the theoretical model to explain the measured anomalous absorption at low frequencies. Previous experiments[10,11] analyzing nonresonant or inversion-line absorption looked at discrete frequencies in the microwave region of the spectrum where the rotational line absorption could be neglected. Over the broad bandwidth of our terahertz system, because of the strength and overlap of the inversion spectrum with the rotational absorption spectrum, the identification and analysis of molecular tunneling is possible only by accurately modeling both spectra and comparing them with the measurements. Therefore in this section we first review the basic relations for calculating the rotational spectra and then present the theoretical background for modeling the inversion spectrum. We then present a unified line-shape theory, which applies for the rotational transitions as well as for the inversion lines. This theory includes the molecular response to an external electric field in the presence of molecular collisions. The resulting new line shape provides an excellent fit to our measurements and avoids contributions from the inversion line to the high-frequency wing of the rotational manifold.

A. Rotational Spectrum

For symmetric top molecules, like the methyl halides, each rotational state with total angular momentum **P** and rotational quantum number J consists of $2J + 1$ sublevels associated with the projection of the angular momentum $\mathbf{P}_z$ on the molecular symmetry axis and indicated by the projection quantum number K. Excitation of the molecules by terahertz radiation induces transitions between pairs of J,K levels of the lowest vibrational state, obeying the selection rules $\Delta J = \pm 1$ and $\Delta K = 0$. The absorption coefficient for such transitions can be calculated as (for details see Ref. 16)

$$\alpha_{JK}(\omega) = \frac{\pi}{3nc\epsilon_0 h}|\mu_{JK}|^2 \times N_{JK}[1 - \exp(-h\omega_{JK}/2\pi kT)] \times \omega g_\alpha(\omega, \omega_{JK}). \quad (1)$$

μ_{JK} is the average dipole matrix element between the rotational states J, K and $J + 1, K$ for unpolarized radiation and/or unoriented molecules (including the transitions from the $2J + 1$ magnetic sublevels) with

$$|\mu_{JK}|^2 = \mu^2 \frac{(J+1)^2 - K^2}{(J+1)(2J+1)}. \quad (2)$$

N_{JK} represents the population per unit volume of the lower rotational state,

$$N_{JK} = \frac{N_a p}{N_a kT + Bp} f_0 \times \frac{S_W(I,K)(2J+1)\exp(-W_{JK}/kT)}{\sum_{J=0}^{\infty}\sum_{K=0}^{J} S_W(I,K)(2J+1)\exp(-W_{JK}/kT)}, \quad (3)$$

determined by the total number of molecules per unit volume (first fraction), the fraction f_0 of molecules in the lowest vibrational state, and the fraction of molecules in the rotational state J,K (second fraction).

In Eq. (1) the term in brackets stands for the difference in the population between the lower and the upper states, and $g_\alpha(\omega, \omega_{JK})$ is a general absorption line-shape function of the form

$$g_\alpha(\omega, \omega_{JK}) = \frac{\Delta\omega_J}{(\omega - \omega_{JK})^2 + (\Delta\omega_J/2)^2} f_\alpha^+ - \frac{\Delta\omega_J}{(\omega + \omega_{JK})^2 + (\Delta\omega_J/2)^2} f_\alpha^-. \quad (4)$$

It differs from the standard Lorentzian form by being multiplied by an additional shape factor, the switching function f_α^+ for the positive resonance term and a similar factor f_α^- for the negative frequency resonance term. For $f_\alpha^\pm = 1$, Eq. (4) is a pure Lorentzian, while for $f_\alpha^\pm = \pm\omega/\omega_{JK}$ it assumes the van Vleck–Weisskopf shape. These switching functions come from molecular response theory[15] and will be discussed in more detail in Subsection 4.C. The width of a line is determined by the collisional dephasing time T_2 equal to the mean time between

collisions, which for further distinction of individual transitions is replaced by $\tau_J = 2/\Delta\omega_J$, where the J-dependent FWHM angular frequency linewidth $\Delta\omega_J$ is assumed to be identical for different K transitions.

The transition frequency is equal to

$$\frac{\omega_{JK}}{2\pi} = 2(J+1)(B_V - D_{JK}K^2) - 4D_J(J+1)^3, \quad (5)$$

and the energy of a J, K level is given by

$$W_{JK} = h[B_V J(J+1) + (A_V - B_V)K^2]. \quad (6)$$

In the preceding equations, n is the nonresonant refractive index, c the speed of light, ϵ_0 the vacuum permittivity, h Planck's constant, μ the permanent electric dipole moment, N_a Avogadro's constant, p the gas pressure, B the virial coefficient correcting the number density of a real gas, kT the thermal energy, $S_W(I, K)$ the statistical weight of a J, K level that is due to spin and K degeneracy, B_V and A_V are the rotational constants of the vibrational state about the total angular momentum and symmetry axis, and D_J and D_{JK} are the respective centrifugal stretching constants. When $B_V h$ and $A_V h$ are small compared with kT, the sums in the denominator of Eq. (3) may be replaced in good approximation by integrals yielding $(4I^2 + 4I + 1)[\pi(kT)^3/B_V^2 A_V h^3]^{1/2}$, where I is the nuclear spin of a hydrogen atom.

The change of the wave vector is given by

$$\Delta k_{JK}(\omega) = \frac{2\pi}{3nc\epsilon_0 h}|\mu_{JK}|^2 N_{JK} \times [1 - \exp(-h\omega_{JK}/2\pi kT)] \times \frac{\omega\omega_{JK}}{\omega_{JK}^2 - \omega^2} g_k(\omega, \omega_{JK}), \quad (7)$$

where $g_k(\omega, \omega_{JK})$ is a general dispersion line-shape function of the form

$$g_k(\omega, \omega_{JK}) = 1 - \frac{\Delta\omega_J^2}{8\omega_{JK}}\left[\frac{(\omega_{JK} + \omega)}{(\omega_{JK} - \omega)^2 + (\Delta\omega_J/2)^2} f_k^+ + \frac{(\omega_{JK} - \omega)}{(\omega_{JK} + \omega)^2 + (\Delta\omega_J/2)^2} f_k^-\right], \quad (8)$$

and $f_k^{\pm}$ are the respective switching functions (presented in Subsection 4.C) of the dispersion.

The rotational absorption $\alpha_r(\omega)$ and dispersion $\Delta k_r(\omega)$ over the spectral range of the terahertz pulse is found by summing over all rotational transitions:

$$\alpha_r(\omega) = \sum_{J=0}^{\infty}\sum_{K=0}^{J} \alpha_{JK}(\omega), \quad (9)$$

$$\Delta k_r(\omega) = \sum_{J=0}^{\infty}\sum_{K=0}^{J} \Delta k_{JK}(\omega). \quad (10)$$

Further details of calculating the absorption, dispersion, and reshaping of the terahertz pulses in the methyl halides have been published previously.[3,15]

B. Inversion Spectrum

To explain the anomalous low-frequency absorption, we now extend the theory developed in the previous subsection to include transitions between states of opposite symmetry. In symmetric top molecules two states of symmetry, + and −, may be distinguished, which represent the two configurations of a molecule with respect to a symmetry or inversion plane. For the methyl halides this plane is defined by the three hydrogen atoms. The carbon-halide group can exist on either side of the plane for some time before it switches to the inverse configuration, and the molecule is turned inside out. The molecule oscillates between both of these states of symmetry owing to tunneling through the high potential barrier. For the case of NH_3 the states are separated by an energy gap such that a transition between them falls in the microwave region; in the case of methyl halides the potential is so high that usually many years are required for an oscillation period, and therefore the inversion frequency is extremely low.

Owing to symmetry each of the rotational states with $K > 0$ is split into a nearly degenerate doublet of inversion levels. Since the selection rules now allow transitions between states with $+ \leftrightarrow -$; $\Delta J = 0, \pm 1$; and $\Delta K = 0$, in addition to the rotational spectrum represented by the $\Delta J = \pm 1$ transitions discussed in the previous subsection, we also observe an additional inversion spectrum designated by transitions $\Delta J = 0$, $\Delta K = 0$, and $+ \leftrightarrow -$ with $K > 0$. Since the energy difference between the inversion levels is negligible the transition frequency between all pairs of adjacent levels is approximately zero, and even at low pressures the linewidth that is due to pressure broadening of such inversion lines is large compared with the center frequency. Only molecular collisions causing an almost continuous broadening of the lines up to frequencies in the far infrared permit monitoring the inversion of molecules as a broad background absorption and dispersion. Note that all J,K levels greater than 0 contribute to this absorption.

With only minimal changes, the calculation of the absorption and dispersion caused by molecular tunneling is performed for the rotational manifold with the same method and equations as in the previous subsection. The dipole transition matrix element μ_{JK} in Eq. (2) is replaced for a $\Delta J = 0$ transition by

$$|\mu_{JK}|^2 = \mu^2 \frac{K^2}{J(J+1)}, \quad (11)$$

and represents the average dipole moment between all magnetic substates for unpolarized radiation and/or randomly oriented molecules. Since the rotational states were considered to be twofold degenerate because of the inversion levels, only half as many transitions may take place between the inversion levels themselves, and thus the statistical weight is a factor-of-2 less. For rotational states with $K = 0$, only one inversion level exists. In this case no inversion transition is allowed, and the summation in Eqs. (9) and (10) over all lines has to start at $J,K = 1$. Finally, we assume a transition frequency $\omega_{JK} = \omega_i \to 0$ and J-independent width $\Delta\omega_i$ of the inversion lines. Since $h\omega_i/2\pi \ll kT$, the difference in the relative populations of the inversion levels given by 1

$-\exp(-h\omega_i/2\pi kT)$ can be well approximated by $h\omega_i/2\pi kT$. Then the power absorption coefficient and phase shift per unit length that is due to inversion take the form

$$\alpha_i(\omega) = \frac{1}{12nc\epsilon_0 kT}\left(\sum_{J=1}^{\infty}\sum_{K=1}^{J}|\mu_{JK}|^2 N_{JK}\right)\omega\omega_i g_\alpha(\omega, \omega_i), \tag{12}$$

$$\Delta k_i(\omega) = \frac{1}{6nc\epsilon_0 kT}\left(\sum_{J=1}^{\infty}\sum_{K=1}^{J}|\mu_{JK}|^2 N_{JK}\right) \times \frac{\omega\omega_i^2}{\omega_i^2 - \omega^2} g_k(\omega, \omega_i), \tag{13}$$

where N_{JK} is the population of a rotational level given by Eq. (3) and $g_\alpha(\omega, \omega_i)$ and $g_k(\omega, \omega_i)$ are the line-shape functions of Eqs. (4) and (8). In calculating the frequency-dependent absorption and dispersion all thermally populated J,K levels contribute to the single spectral feature, owing to the inversion line at zero frequency. In our calculations the maximum values of J and K were $J,K = 75$ for methyl chloride and $J,K = 50$ in methyl fluoride.

In a semiclassical picture this absorption and dispersion can be explained through the reorientation of a dipole moment parallel to the total-angular-momentum vector **P**. In a symmetric top molecule the full dipole moment, which is directed along the molecular symmetry axis $\mathbf{P}_z$, can be resolved into components parallel and perpendicular to **P**. While the perpendicular component rotates with ω_{JK} and is responsible for the rotational spectrum, the parallel component switches with the inversion frequency from the parallel to the antiparallel orientation or vice versa and thus determines the inversion spectrum. The respective quantum-mechanical dipole transition matrix elements for these two components are given in Eqs. (2) and (11). Quite similar relations can also be found when considering a classical rotator with a quantum-mechanical angular momentum $P_z = Kh/2\pi$ along the symmetry axis and a total angular momentum $P = [J(J+1)]^{1/2}h/2\pi$. In this context it should be noticed that in linear molecules the angular momentum along the symmetry axis is zero, and any dipole component parallel to **P** disappears. Therefore linear molecules do not show absorption that is due to molecular tunneling.

C. Line-Shape Considerations

The overall absorption and dispersion across the whole spectrum probed in our measurement are determined by the linewidth and shape of the transitions, which contain information on the collision behavior as well as on the intermolecular forces. For the higher frequencies of optical and infrared transitions, it is well known that the simple Lorentzian line shape[17] provides excellent agreement with experiment, particularly for the central region of the line. As the frequencies are reduced to those of the microwave or far-infrared region, and under conditions when a linewidth becomes comparable to the transition frequency, the absorption profile of a collision-broadened line is better represented by a van Vleck–Weisskopf line shape.[18] Also for the limiting case of zero-transition frequency the absorption and dispersion is described by the van Vleck–Weisskopf theory, which then converges to the Debye theory, while the Lorentzian theory is not applicable at these frequencies.

The difference between the Lorentz and the van Vleck–Weisskopf theories is that the response of a molecule to an external field is considered only in its two limiting cases. While Lorentz assumed that, directly after a collision, molecules are oriented randomly with respect to the driving field and therefore no macroscopic polarization in the sample will be found,[17] van Vleck and Weisskopf applied Boltzmann's statistics,[18] assuming instantaneous realignment during a collision such that the molecules are oriented to have low energy in the field. A distribution in accordance with the Boltzmann law can be expected when the collision duration is short compared with the period of oscillation of the field. This is known as the adiabatic hypothesis in the van Vleck–Weisskopf theory.[18] However, when the oscillations of the field become faster than the collision duration time or faster than any time response of molecules to the impressed field, thermalization cannot be established over the collision, and the original approximation of Lorentz becomes more realistic.

The frequency range over which the transition between the two theories occurs indicates the duration of the collision or the molecular response time τ_C. This frequency range is completely covered by the spectrum of the terahertz pulses and therefore can be investigated by THz-TDS.

It is obvious that a more inclusive line-shape theory, which is applicable over the full spectral range, must include the temporal response of molecules to the field. We have derived such a molecular-response theory[15] for rotational transitions, but the theory is also applicable to the inversion spectrum. Inclusion of the molecular response results in a time-dependent and therefore also frequency-dependent extra polarization of the vapor, which may be formed over the collision duration time. This extra polarization results from the tendency of molecules to orient their dipole moment parallel to the field, as was considered in the van Vleck–Weisskopf case, but in molecular-response theory the orientation is not assumed to be instantaneous. In the frequency domain the magnitude of this extra polarization is determined by the frequency detuning of the field from the transition frequency compared with the reciprocal of the molecular-response time τ_C. The polarization can vary from zero at high-frequency detunings (Lorentz case) to a maximum polarization representing thermal equilibrium at low-frequency detunings (van Vleck–Weisskopf case). Since in a symmetric top molecule the dipole moment can be separated into the two components parallel and perpendicular to the total angular momentum, two components of the extra polarization must also be distinguished, with the perpendicular part contributing to the rotation spectrum and the parallel part to the inversion spectrum.

These extra polarizations modify the absorption and dispersion of the vapor giving rise to small corrections in the wing of a spectral line. The faster the response of molecules, the more these contributions are shifted to the

far wing of a line up to the limit of instantaneous response, which is the van Vleck–Weisskopf case. From molecular response theory[15] we find a generalized line shape of the type given by Eq. (4) for the absorption and by Eq. (8) for the dispersion. The switching function for absorption assumes the form

$$f_\alpha^{\pm}(\omega, \omega_{JK}) = 1 - \frac{\omega_{JK} \mp \omega}{\omega_{JK}} \frac{1 + \Delta\omega_J \tau_C/2}{1 + (\omega_{JK} \mp \omega)^2 \tau_C^2}, \tag{14}$$

while that for the dispersion is given by

$$f_k^{\pm}(\omega, \omega_{JK}) = 1 - \frac{\omega_{JK} \mp \omega}{\omega_{JK}} \frac{1 - 2(\omega_{JK} \mp \omega)^2 \tau_C/\Delta\omega_J}{1 + (\omega_{JK} \mp \omega)^2 \tau_C^2}, \tag{15}$$

where τ_C is the molecular response time. These functions control the transition between the two basic line shapes and describe the admixture of a van Vleck–Weisskopf profile to a Lorentzian as a function of the frequency detuning from resonance. An inspection of the switching functions shows that in the limit $(\omega_{JK} \mp \omega)^2 \tau_c^2 \gg 1$, $f_\alpha^{\pm} \to 1$, and the generalized line-shape function becomes the well-known Lorentzian for absorption, while $f_k^{\pm} \to 1 + (\omega_{JK} \mp \omega)\tau/\omega_{JK}\tau_C$. Conversely, when $(\omega_{JK} \mp \omega)^2 \tau_C^2 \ll 1$, $f_{k,\alpha}^{\pm} \to \pm\omega/\omega_{JK}$, and the van Vleck–Weisskopf line shape is obtained. Figure 6 shows the switching function of the positive resonance term of the absorption for the $J = 35$ transition in methyl chloride with resonance frequency ω_{JK} near 1 THz, a linewidth $\Delta\omega_J = 25$ GHz, and a response time $\tau_C = 220$ fs.

It has to be emphasized that the line shapes and switching functions for both the rotational lines as well as the inversion lines are the same, as long as the transition frequencies ω_{JK} and ω_i have finite values. The reason for this is that both spectra are underlying the same physical mechanisms with an identical molecular response for the parallel and the perpendicular components of the extra polarization.

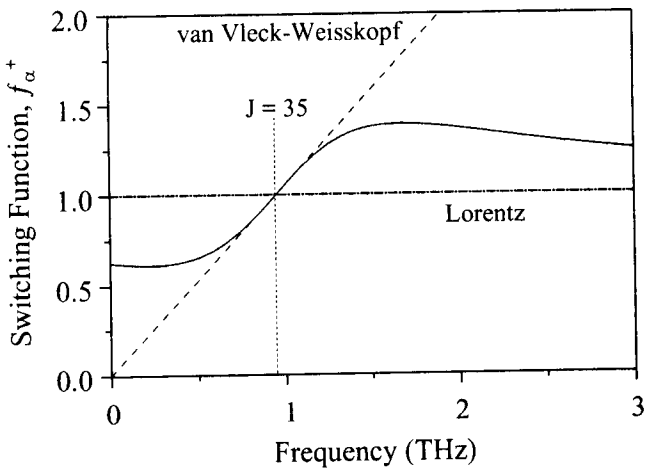

Fig. 6. Switching function (solid curve) of the positive resonance term of the absorption for a transition in methyl chloride with $J = 35$, a resonance frequency ω_{JK} of ~1 THz, a linewidth $\Delta\omega_J = 25$ GHz, and a response time $\tau_C = 220$ fs. The switching function in the van Vleck–Weisskopf and Lorentz limits is also shown.

For the limiting case of $\omega_{JK} = \omega_i = 0$ it is necessary to first consider the limits of the absorption coefficient and phase change per unit length to avoid division by zero in the denominators of Eqs. (14) and (15). Then the absorption and dispersion that are due to inversion assume the forms

$$\alpha_i(\omega) = \frac{1}{3nc\epsilon_0 kT} \left(\sum_{J=1}^{\infty} \sum_{K=1}^{J} |\mu_{JK}|^2 N_{JK} \right) \omega g_\alpha^i(\omega), \tag{16}$$

$$\Delta k_i(\omega) = \frac{1}{6nc\epsilon_0 kT} \left(\sum_{J=1}^{\infty} \sum_{K=1}^{J} |\mu_{JK}|^2 N_{JK} \right) \omega g_k^i(\omega), \tag{17}$$

with the new line-shape functions for $\omega_i = 0$:

$$g_\alpha^i(\omega) = \frac{\omega\tau_i}{1 + \omega^2\tau_i^2} f_\alpha^i(\omega), \tag{18}$$

$$g_k^i(\omega) = \frac{1}{1 + \omega^2\tau_i^2} f_k^i(\omega), \tag{19}$$

and the shape factors

$$f_\alpha^i(\omega) = \frac{1 + \tau_C/\tau_i}{1 + \omega^2\tau_C^2}, \tag{20}$$

$$f_k^i(\omega) = \frac{1 - \omega^2\tau_C\tau_i}{1 + \omega^2\tau_C^2}, \tag{21}$$

where $\tau_i = 2/\Delta\omega_i$. When $\omega\tau_C \ll 1$, $f_{\alpha,k}^i \to 1$, the line-shape functions in Eqs. (18) and (19) become the standard Debye equations for absorption and dispersion. With increasing frequency, however, particularly when $\omega\tau_C > 1$, a completely different absorption and dispersion behavior than expected from the standard equations is found. This different behavior originates from the inclusion of the response of molecules to the impressed field. The underlying theory naturally avoids the physically unrealistic situation of a constant absorption, the so-called Debye plateau, at higher frequencies.

Assuming the form $\chi(\omega) = \chi'(\omega) - i\chi''(\omega)$ for the complex electric susceptibility, the phase shift and power absorption are $\Delta k(\omega) = (k_o/2n^2)\chi'(\omega)$ and $\alpha(\omega) = (k_o/n^2)\chi''(\omega)$, respectively, where $k_o = \omega n/c$ is the nonresonant wave vector in the sample. From Eqs. (16)–(21) we can write the susceptibility determined by molecular-response theory in the relatively simple form

$$\chi(\omega) = \frac{1}{3c\epsilon_0 kT} \left(\sum_{J=1}^{\infty} \sum_{K=1}^{J} |\mu_{JK}|^2 N_{JK} \right) \times \frac{1}{1 + i\omega\tau_i} \frac{1}{1 + i\omega\tau_C}. \tag{22}$$

It is important to note that the complex terms of the form $A(\omega) = 1/(1 + i\omega\tau)$ satisfy the Kramers–Kronig relationship[19] and are the frequency-domain representation of the time-domain response function $\exp(-t/\tau)$, which vanishes for positive argument as required by causality. This relationship describes both the dielectric Debye[14] and the conductive Drude[20] response. Equation

(22) shows a product of two of such frequency-domain functions corresponding to the time-domain response functions of the collision process $\exp(-t/\tau_C)$ and the dephasing process between collisions $\exp(-t/\tau_i)$, both of which vanish for positive argument. The complete result for $\chi(\omega)$ also satisfies the Kramers–Kronig relationship and is fully consistent with linear response theory. The form of $\chi(\omega)$ is similar to that of the two-parameter Rocard–Powles complex permittivity,[21–23] which is the next-higher-order approximation after the single-parameter Debye theory.

Indeed, in the zero-resonance-frequency limit considered here, molecular-response theory has the same mathematical form as the Rocard–Powles result, which was derived by the inclusion of nonzero molecular inertia into the Debye theory.[21–23] This form of the complex susceptibility is the same as that obtained by a second-order truncation of the Mori continued fraction.[23] Thus the transition dipole autocorrelation function has a maximum at $t = 0$ with zero slope, which can be seen in Fig. 7 by plotting the susceptibility, $\chi(\omega)$ of Eq. (22), on a Cole–Cole plot, which shows the imaginary part of $\chi(\omega)$ plotted against the real part. In the high-frequency limit this curve asymptotically approaches the real axis, indicating the correct behavior of the dipole autocorrelation function near zero time.[23] Although the second-order truncation of the Mori continued fraction is an approximation, the experimental results clearly indicate the validity of molecular response theory over this frequency range.

From a semiclassical viewpoint we can compare the absorption and dispersion given in Eqs. (16) and (17) with the classical results of Debye,[14] who considered the nonresonant absorption of radiation interacting with dipoles in a viscous medium. In a gas the analog to Debye's treatment is to consider molecules with an inertia large enough that they can be regarded as stationary between collisions (i.e., the collision frequency is high compared with the molecular-rotation frequency) and assuming an average orientation of the molecular dipoles to the field in accordance with Boltzmann's law.[18] This orientation exactly represents the extra polarization discussed above, which in the case of a symmetric top can be separated into the perpendicular and parallel components. Therefore, in the limit of $\omega_{JK} \ll \Delta\omega_J$ and $\omega_i \ll \Delta\omega_i$, the sum of the absorptions given by Eq. (1) for the rotation and by Eq. (16) for the inversion represent the quantum-mechanical form of the classical Debye absorption. Similarly, Eqs. (7) and (17) give the resulting dispersion.

In the case of $\omega_{JK} > \Delta\omega_J$ and $\omega_i > \Delta\omega_i$ and particularly at an angular frequency ω of the field, which is close to or in resonance with a transition, the extra polarizations and therefore those contributions that directly relate to the Debye case and describe the nonresonant behavior are completely covered by the much stronger resonant contributions. They can be observed only in the far wing of the lines.

Since in methyl halides the inversion frequency is essentially zero, the parallel dipole moment is almost stationary in space. A transition to the inverse configuration and therefore a reorientation of the dipoles will then be observed only because of molecular collisions. In the presence of an electric field the preferred transitions that take place are those that increase the dipole moment in the direction of the field, and consequently the vapor becomes polarized. However, this polarization is of the same type as the orientation of dipoles that are due to collision-induced transitions between magnetic sublevels contributing to the Debye absorption. Therefore, in the limit of zero inversion frequency, both contributions become indistinguishable and Eqs. (16) and (17) can also be interpreted as Debye-type absorption and dispersion originating from the dipole moment parallel to the angular momentum **P**.

In methyl halides the magnitude of the absorption that is due to the parallel component of the angular momentum vector is typically one order of magnitude smaller than that of the resonant contribution of the dipole moment perpendicular to the angular momentum vector. However, since the Debye-type absorption of the perpendicular component underlies the rotational resonance structure, this term is shifted with the rotational transitions to higher frequencies, and in the low-frequency range, up to 100 GHz, both contributions are of comparable magnitude.

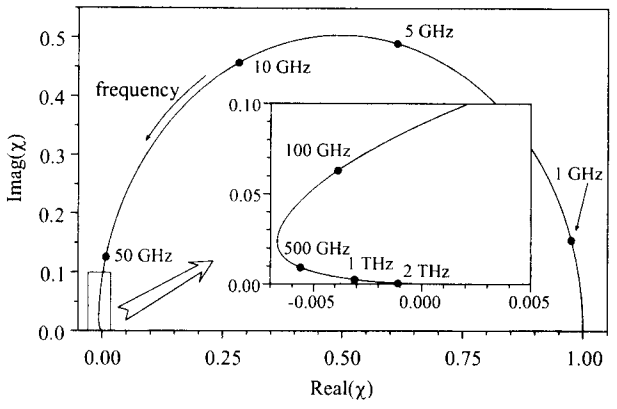

Fig. 7. Cole–Cole plot of the electric susceptibility $\chi(\omega)$ of the molecular-response theory with the time between collisions $\tau = 25$ ps and molecular-response time $\tau_C = 0.2$ ps. Frequency increases counterclockwise with discrete frequency points from 1 GHz to 2 THz, marked as filled circles.

5. DISCUSSION OF RESULTS

An analysis of the measurements presented in Section 3 was performed by Fourier transforming the measured pulse structures into the frequency domain and comparing them with theoretical spectra. Additionally, the analysis was done in the time domain by simulating the pulse structures and comparing them directly with the measurements. In both cases, first the absorption and dispersion of the vapor have to be calculated with the known molecular constants by means of the theoretical framework presented in the previous section. Multiplication of these spectra with the Fourier transform of the input pulse gives the transmitted amplitude absorption and dispersion spectrum behind the vapor. The inverse numerical Fourier transform of the calculated absorption and dispersion spectra yield the predicted output pulses transmitted through the vapor.

To successfully fit our experimental results, we must address the three aspects of the theory developed in Section 4. The first parameter that must be determined is the collision broadening of the rotational lines and their influence on the far wings of the spectrum. The second is to obtain the line shape of the rotational lines and from this, the molecular response or orientation time τ_C, used in the theory of Subsection 4.C. The third aspect, forced by the experimental results presented here, is to identify the contribution originating from molecular tunneling and then to determine the collisional broadening of the inversion lines.

The line broadening is determined by a measurement of the type shown in Fig. 2, which uses a spectrally broad input pulse and a short cell length that permit observation of the linewidth broadening over the entire rotational band manifold. At pressures of 2 atm (2026 hPa) or more the individual lines are severely broadened and almost completely overlapping, as seen in Fig. 2(c). Despite the strong broadening we do not lose information at the center of the band when the vapor becomes opaque as with longer path lengths, and we are still able to measure a variation of the linewidth with rotational quantum number J. This is observable as a lower resolution between the broader lines at the low-frequency side and the stronger modulation between lines appearing at the high-frequency side of the absorption band.

For a quantitative analysis of such measurements the experimental absorption is directly compared with the theoretical amplitude absorption $\alpha(\omega)L/2$, obtained with the method outlined in Subsection 4.A. Figure 8(a) shows the measured absorption (solid curve) together with that calculated (dashed curve) for 2000 hPa of methyl chloride and a cell length $L = 2.27$ cm. The measurement and calculation overlap completely except at the lowest frequencies. A fit of the theoretical spectrum to the measurement yields the J-dependent distribution of the pressure broadening coefficient shown in Fig. 8(b). This distribution is important to extract the contribution of the rotational band at the low-frequency side of the spectrum and to determine the line shape with the molecular response time from the remaining absorption at the high-frequency wing.

The 2.27-cm cell is too short to allow observation of small changes in the far-wing absorption from which we obtain detailed information on the line shape. However, on the low- and high-frequency wings, these contributions can be measured by use of the much longer 38.2-cm vapor cell, since the absorption $\alpha(\omega)L/2$ increases linearly, and the transmitted signal through the vapor decreases exponentially with increasing cell length. Figure 3 represents such a measurement, where we used the long cell filled with 3039 hPa of methyl chloride. At the center of the band the vapor is opaque, but the transmitted spectral components, shown in Fig. 3(b), are very sensitive to the remaining absorption, which is determined mainly by the far wings.

Comparison with a theoretical spectrum shows that the measurements are well fit by means of a van Vleck–Weisskopf line shape for an individual transition out to frequency offsets of the order of 1 THz. However, further increasing the offset leads to a reduced absorption at the high-frequency side of Fig. 3(b) of the order of two compared with that of the van Vleck–Weisskopf line shape. These discrepancies completely disappear when the generalized line-shape function given by Eqs. (4) and (14) is applied. A calculation of absorption considering only the rotational manifold is shown in Fig. 3(b) (dashed curve) together with the measurement (solid curve). The good agreement at the high-frequency side of the spectrum is obtained with a molecular-response time of $\tau_C = 220$ fs.

The observed deviation between our measurements and theory in the low-frequency wing [Fig. 3(c)] results from the additional contribution originating from molecular tunneling. The previously unexplained deviation is seen more clearly in the methyl chloride data of Fig. 4, for which the terahertz system was optimized for low frequencies. Similar discrepancies are seen in Fig. 5 for long-path-length data on methyl fluoride.

By including the additional absorption, derived in Subsection 4.B and due to zero-frequency transitions between inversion states, the results shown in Fig. 9 are obtained. This calculation is a superposition of the inversion spectrum [Eq. (16)] and the rotation spectrum [Eq. (9)], where we assumed the same molecular response and time constant for both spectra. Figure 9(a) is the same measurement as that shown in Fig. 3(b) (3039 hPa of methyl chloride) with the inversion lines included in the calculation. The inset shows the low-frequency wing on an expanded scale. The discrepancy seen in Fig. 3(c) is completely removed.

The improved fits to the low-frequency wing can be seen more clearly in the measurement of 5512 hPa of me-

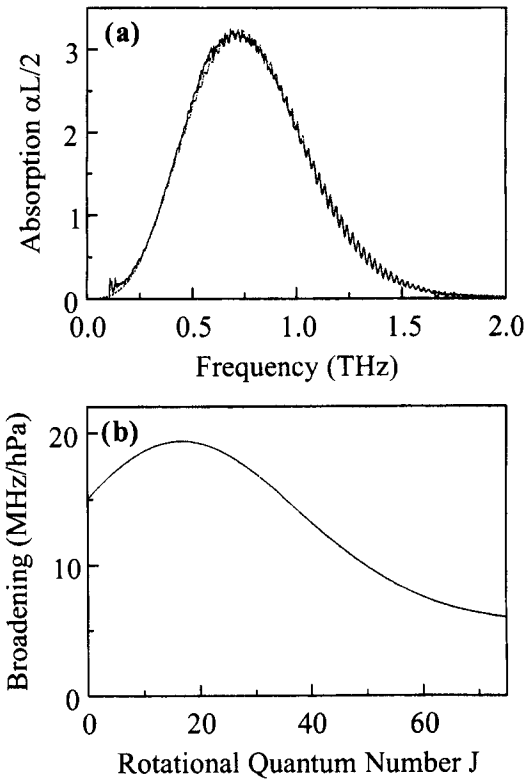

Fig. 8. (a) Measured (solid curve) and calculated absorption (dashed curve) for 2000 hPa of methyl chloride and a cell length of 2.27 cm. (b) J-dependent linewidth distribution of the rotational spectrum.

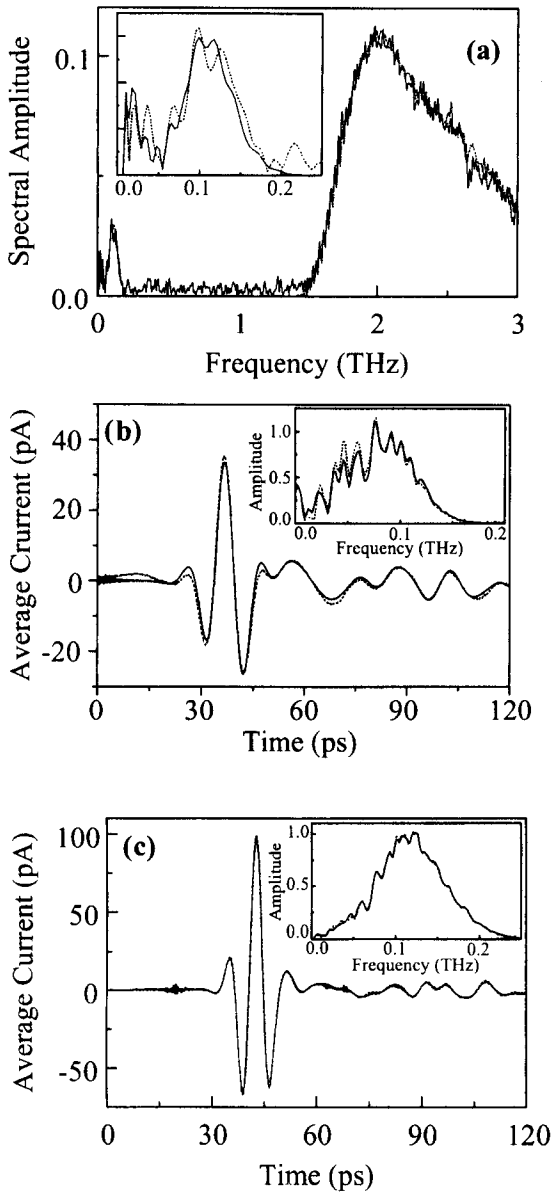

Fig. 9. (a) Fourier transform of the measured transmitted pulse (solid curve) through 3039 hPa of methyl chloride vapor [see also Fig. 3(b)] and calculation (dashed curve) including the inversion spectrum. The inset shows the low-frequency wing. (b) Measurement (solid curve) and calculation with inversion line absorption (dashed curve) of the transmitted pulse in 5512-hPa methyl chloride vapor. The inset shows the amplitude spectrum. (c) Measurement (solid curve) and calculation with inversion line absorption (dashed curve) of the transmitted pulse in 4059-hPa methyl fluoride vapor. The inset shows the amplitude spectra, which completely overlap.

thyl chloride from Fig. 4, with the system tuned to low frequencies. Figure 9(b) shows the measured transmitted terahertz pulse shape of Fig. 4(b) with the fit, by means of the molecular response line shape and including the inversion lines, overlaid as a dashed curve. The corresponding spectra are in the inset. The absorption measured on the low-frequency wing is stronger than expected and is now well explained by the theory.

Figure 9(c) shows the 4059-hPa methyl fluoride measurement of Fig. 5, including the zero-frequency inversion transition. The measurement (solid curve) and calculation (dashed curve) now agree for both the transmitted pulse shape and the spectra shown in the inset to the figure.

For all the measurements shown in Fig. 9 the fits, which include the inversion line and modified line shape, are excellent. Note that although the peak absorption that is due to the overlapping inversion lines is up to one hundred times smaller than the maximum rotational absorption (therefore the transmitted signals differ by more than 40 orders of magnitude), the contribution originating from the inversion can well be distinguished from the wing absorption of the rotational band.

All the fits of Fig. 9 corresponding to terahertz transmission on the low-frequency wings were obtained with the line shape developed in Subsection 4.C. The inversion line shape obtained from the molecular response theory does not affect the absorption on the high-frequency wing. In contrast, application of the classical Debye line shape to the inversion spectrum produces an inadmissible large extra absorption at the high-frequency side of the spectrum, which is in contradiction to the observations. Figure 10 compares the absorption and dispersion of the Debye case (upper dashed curves) with those found from Eqs. (16)–(21) (lower solid curves) for a response time τ_C = 220 fs. While the Debye theory predicts a nonphysical broad, constant absorption [Fig. 10(a)] and flat phase shift [Fig. 10(b)] at the higher frequencies, which is nonphysical, molecular-response theory predicts an absorption with a well-restricted maximum at 150 GHz, and the dispersion essentially is concentrated at the low-frequency range. At a given pressure and propaga-

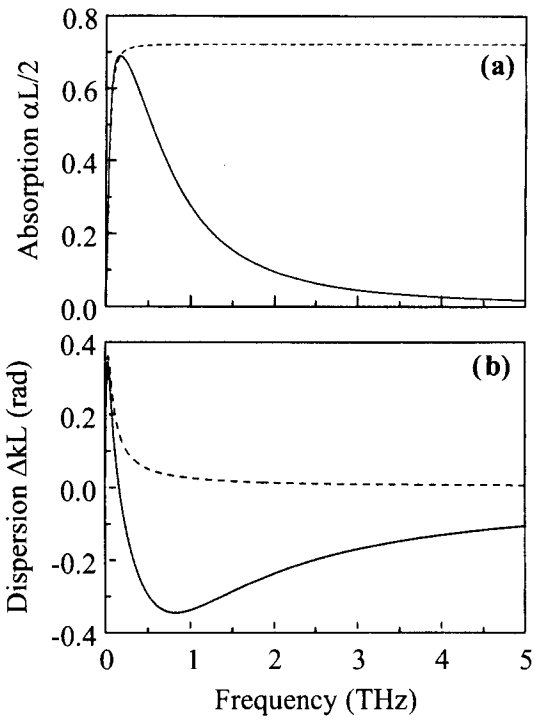

Fig. 10. (a) Calculated absorption and (b) dispersion of the inversion spectrum by use of the Debye theory (dashed upper curves) and the new line-shape theory (solid lower curves) for 3039 hPa of methyl chloride with C_i = 13 MHz/hPa and τ_C = 220 fs.

tion length (here, $p = 3039$ hPa of methyl chloride, $L = 38.2$ cm) the absolute absorption strength and phase shift is controlled only by the pressure-broadened width of the inversion lines. From the fit to the methyl chloride measurements in Figs. 9(a) and 9(b), we obtain a broadening parameter $C_i = 13$ MHz/hPa, which is defined by the relation $\Delta\omega_i = 2/\tau_i = 2\pi C_i p$ and agrees well with the broadening of the rotational lines at the low-frequency side of the spectrum. Fitting to the transmitted terahertz pulse and corresponding spectrum in Fig. 9(c) for 4059 hPa of methyl fluoride yield a molecular-response time of $\tau_C = 190$ fs and a broadening parameter of $C_i = 10$ MHz/hPa.

These results agree well with the results of Walter and Hirshberger[10] but show some deviations with respect to those of Bleany and Loubser.[11] The main difference between our measurements and the older data is that the terahertz experiments continuously cover the inversion spectrum as well as the rotation spectrum and therefore allow for observations over a wide spectral range, while the microwave experiments[10,11] were restricted to fixed frequencies within a limited frequency range. The broad spectrum measured by means of terahertz spectroscopy makes it possible to distinguish our new line shape from the standard Debye (or zero-frequency-limit van Vleck–Weisskopf), since earlier microwave measurements could not measure the high-frequency far wing of the rotational manifold.

The excellent agreement between measurements and calculation confirms our interpretation of the small absorption in the low-frequency wing of the terahertz spectrum as molecular tunneling in methyl halides. The presented results demonstrate the significance of molecular-response theory for the low-frequency range and its application in the zero-frequency limit to overcome the nonphysical high-frequency absorption of the Debye theory.

6. CONCLUSION

Using the powerful technique of THz-TDS, we have experimentally and theoretically studied the absorption and dispersion of methyl halide vapors. Our measurements showed small deviations in the low-frequency wing of the rotational spectra, which originate from molecular tunneling. We have expanded our new molecular-response theory to apply to the inversion lines, including the limiting case of zero-transition frequency. This line-shape theory, originally developed for the rotation spectrum, includes the molecular response of polar molecules to an external electric field over the duration of a collision. It unifies the basic collision theories of Lorentz, van Vleck and Weisskopf, and Debye, where the molecular-response time τ_C acts as the control parameter. The calculated absorption and dispersion based on this theory fits the measurements over the full spectral range of the terahertz spectrum. The response time τ_C is found to be of the order of 200 fs, causing an inversion absorption with a well-restricted maximum at 150 GHz.

ACKNOWLEDGMENTS

We acknowledge financial support by NATO (H. Harde and D. Grischkowsky) under grant CRG 941172 and by the National Science Foundation (R. A. Cheville and D. Grischkowsky) under grant PHY-9422952.

REFERENCES

1. H. Harde, S. Keiding, and D. Grischkowsky, "THz commensurate echoes: periodic rephasing of molecular transitions in free-induction decay," Phys. Rev. Lett. **66**, 1834 (1991).
2. H. Harde and D. Grischkowsky, "Coherent transients excited by subpicosecond pulses of terahertz radiation," J. Opt. Soc. Am. B **8**, 1642 (1991).
3. H. Harde, N. Katzenellenbogen, and D. Grischkowsky, "Terahertz coherent transients from methyl chloride vapor," J. Opt. Soc. Am. B **11**, 1018 (1994).
4. H. Harde, N. Katzenellenbogen, and D. Grischkowsky, "Line-shape transition of collision broadened lines," Phys. Rev. Lett. **74**, 1307 (1995).
5. M. van Exter, Ch. Fattinger, and D. Grischkowsky, "High brightness terahertz beams characterized with an ultrafast detector," Appl. Phys. Lett. **55**, 337 (1989).
6. M. van Exter, Ch. Fattinger, and D. Grischkowsky, "Terahertz time-domain spectroscopy of water vapor," Opt. Lett. **14**, 1128 (1989).
7. M. van Exter, Ch. Fattinger, and D. Grischkowsky, "Time-domain far-infrared spectroscopy of water vapor and direct measurement of collisional relaxation times," in *Laser Spectroscopy IX—Proceedings of the Ninth International Conference on Laser Spectroscopy*, M. S. Feld, J. E. Thomas, and A. Mooradian, eds. (Academic, San Diego, Calif., 1989).
8. D. Grischkowsky, S. Keiding, M. van Exter, and Ch. Fattinger, "Far-infrared time-domain spectroscopy with terahertz beams of dielectrics and semiconductors," J. Opt. Soc. Am. B **7**, 2006 (1990).
9. M. van Exter and D. Grischkowsky, "Characterization of an optoelectronic terahertz beam system," IEEE Trans. Microwave Theory Tech. **38**, 1684 (1990).
10. J. E. Walter and W. D. Hershberger, "Absorption of microwaves by gases. II," J. Appl. Phys. **17**, 814 (1946).
11. B. Bleaney and J. H. N. Loubser, "The inversion spectrum of NH_3, CH_3Cl, and CH_3Br at high pressures," Proc. Phys. Soc. London, Sec. A **63**, 483 (1949).
12. G. Birnbaum, "Theory of microwave nonresonant absorption and relaxation in gases," Phys. Rev. **150**, 101 (1966).
13. N. Katzenellenbogen and D. Grischkowsky, "Efficient generation of 380 fs pulses of THz radiation by ultrafast laser pulse excitation of a biased metal-semiconductor interface," Appl. Phys. Lett. **58**, 222 (1991).
14. P. Debye, *Polar Molecules* (Chemical Catalog, New York, 1929) Chap. 5.
15. H. Harde, R. A. Cheville, and D. Grischkowsky, "THz studies of collisionally broadened rotational lines," J. Phys. Chem. A **101**, 3646 (1997).
16. C. H. Townes and A. L. Schawlow, *Microwave Spectroscopy* (Dover, New York, 1975).
17. H. A. Lorentz, Proc. Amst. Akad. Sci. **8**, 591 (1906).
18. J. H. van Vleck and V. F. Weisskopf, "On the shape of collision broadened lines," Rev. Mod. Phys. **17**, 227 (1945).
19. R. L. Kronig, "On the theory of dispersion of x-rays," J. Opt. Soc. Am. **12**, 547 (1926); H. A. Kramers, Atti Congr. Intern. Fis. **2**, 545 (1927).
20. P. Drude, "Bestimmung der optischen Contanten der Metalle," Ann. D. Physik **39**, 504 (1890).
21. M. Y. Rocard, "Analyse des orientation moleculaires de molecules a moment permanent dans un champ alternatif application a la dispersion de la constante dielectrique et a l'effet Kerr," J. Phys. Radium **4**, 247 (1933).
22. J. G. Powles, "The effect of molecular inertia on dielectric absorption," Trans. Faraday Soc. **48**, 802 (1948).
23. G. W. Chantry, "Properties of dielectric materials," in *Infrared and Millimeter Waves* (Academic, New York, 1983), Vol. 8.